Inorganic Chemistry

pubs.acs.org/IC
Article

Expanding the Toolbox: Synthesis of Zintl Salts Containing Anions of the In/Sb and Tl/Sb Elemental Combinations

Katrin Beuthert, Nils Spang, Diana Carolina Alzate Millan, Lukas Guggolz, and Stefanie Dehnen*

Cite This: *Inorg. Chem.* 2025, 64, 8711−8718

ABSTRACT: Binary Zintl anions comprising atoms of two p-block elements, and ternary Zintl clusters, in which the latter are combined with d-/f-block metal ions, are being studied with great activity. However, although an impressive variety of elemental compositions have been realized, some combinations of the p-block (semi)metals are lacking in corresponding substructures. The In/Sb combination is extremely rare, and Tl/Sb has not yet been realized at all, although the existence of *pseudo*-tetrahedral species, for instance, was predicted by quantum chemical studies. Extraction of the novel ternary phase K_6InSb_3 and of $K_6Tl_2Sb_3$ with ethane-1,2-diamine (en) yielded binary Zintl anions of these elemental combinations as salts comprising *pseudo*-tetrahedral anions $(InSb_3)^{2-}$ and $(TlSb_3)^{2-}$ or nine-vertex cages $(In_4Sb_5)^{3-}$ and $(Tl_4Sb_5)^{3-}$, respectively. To establish efficient synthesis routes, the extractions were monitored using electrospray-ionization mass spectrometry and fractionated crystallization. We thereby isolated salts of two further anions that might represent intermediates on the way to larger species, namely, a novel salt of the Sb_7^{3-} anion, and a salt of the new binary anion $(TlSb_7)^{2-}$. We describe the experimental approach, the process of its optimization, the geometric structures of the new compounds as well as their electronic structures that were established by DFT calculations.

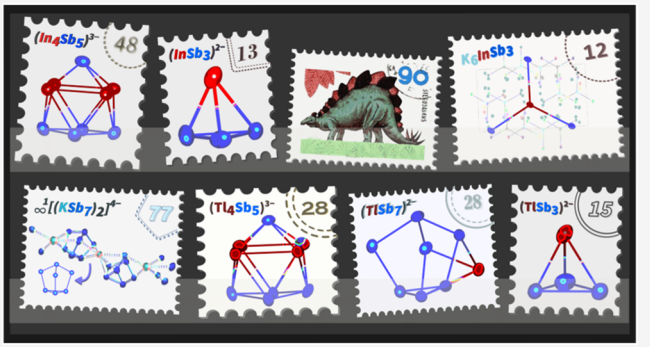

INTRODUCTION

The investigation of yet unexplored combinations of p-block elements in binary Zintl anions has been of great interest for the establishment and efficient access of novel multimetallic Zintl clusters in the recent past. Such compounds not only challenge our understanding of chemical bonding and provide insights into the formation of cluster molecules in general, but also show an untapped potential in the pursuit of previously unknown intermetallic solids and nanomaterial morphologies, and in opening several new avenues toward further application-based studies.[1,2] Recent results show that it is possible to use Zintl clusters in homogeneous catalysis,[3] access impressive cluster architectures like $[K(2,2,2\text{-crypt})]_5[K@Au_{12}Sb_{20}]$,[4] and realize and explore very uncommon intermetallic bonding modes.[5]

The most common starting point for the use of binary Zintl anions in follow-up chemistry is found in *pseudo*-tetrahedral anions of the form $(TrPn_3)^{2-}$ and $(Tt_2Pn_2)^{2-}$ (where Tr is a group 13 element, Tt is a group 14 element, and Pn is a group 15 element). However, of all the theoretically possible combinations of p-block (semi)metals, a considerable number are yet to be synthetically realized, although quantum chemical calculations predicted several of them to be stable.[6] The reason as to why only some of them seem to be accessible experimentally has been put down to a preferrable combination of atomic sizes and electron affinities of the elements involved (Scheme 1), as this reduces interatomic strain. In addition, this is a phenomenological rationale based on previous observations. According to these predictions, *pseudo*-tetrahedral anions should be accessible if (a) the corresponding figures fall within the given limits and if (b) corresponding synthetic approaches can be established.

Although some element combinations might theoretically be possible, it remains a significant challenge to fill in the gaps synthetically. This is mainly due to the lack of appropriate intermetallic precursors required for corresponding extraction experiments that ultimately afford the *pseudo*-tetrahedral anions. Hence, for expansion of the library of binary Zintl anions, the development of a toolbox for the synthesis of such *pseudo*-tetrahedral precursors for follow-up reactions toward larger cluster architectures is required.

Some of the *pseudo*-tetrahedral Zintl anions can be obtained in high-yield and high-purity salts on a multigram scale, e.g., $(Sn_2Sb_2)^{2-}$ or $(InBi_3)^{2-}$.[7,8] However, this does by far not apply

Received: February 15, 2025
Revised: March 14, 2025
Accepted: March 20, 2025
Published: April 21, 2025

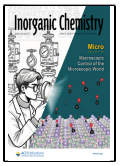

https://doi.org/10.1021/acs.inorgchem.5c00724
Inorg. Chem. 2025, 64, 8711−8718

Scheme 1. Overview of Ratios of Covalent Radii[6] (Q_{cr}) of Elements Tr, Tt and Pn in *Pseudo*-Tetrahedral Anions $(TrTt_3)^{5-}$, $(TrPn_3)^{2-}$, and $(Tt_2Pn_2)^{2-}$ (Tr: Group 13 Element, Tt: Group 14 Element, Pn: Group 15 Element)[a]

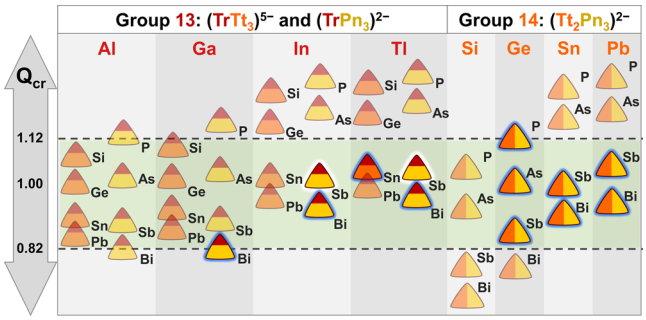

[a]The dashed lines indicate the suggested lower and upper limit of ratios for species to be accessible, according to known species isolated in corresponding salts. Still unknown species are drawn in semi-transparent mode. Eleven tetrahedra, indicated by blue highlight, have been previously known, the two ones with white highlight are being added in this work.

to all other elemental combinations. Most of them, e.g., $(TlBi_3)^{2-}$ and $(Ge_2Sb_2)^{2-}$,[9,10] cannot be isolated in high yield without the formation of byproducts, while other elemental combinations have not been accessible at all. The combination of Tl and Sb in a Zintl compound is one of them. For In and Sb, only one species based on a binary In/Sb structure has been reported to date, $[K([2.2.2]crypt)]_4[In_8Sb_{13}]$. It has been synthesized by a reaction of K_5Sb_4 with $[In(benzyl)_3]$ in ethane-1,2-diamine (en) in the presence of 4,7,13,16,21,24-hexaoxa-1,10-diazabicyclo[8.8.8]hexacosane (crypt-222).[11]

Here, we report a systematic and atomically precise approach toward a salt comprising the elusive $(InSb_3)^{2-}$ anion by oxidative extraction of the new intermetallic solid K_6InSb_3 in en/crypt-222. A similar approach yielded a salt of the slightly more oxidized anion $(In_4Sb_5)^{3-}$. Salts of the equally elusive heavier congeners, $(TlSb_3)^{2-}$ and $(Tl_4Sb_5)^{3-}$, resulted from extraction of the known phase $K_6Tl_2Sb_3$.[12] These procedures additionally afforded a new salt of the Sb_7^{3-} anion and a yet unknown binary expansion of it, $(TlSb_7)^{2-}$, both of which can be viewed as intermediates during the formation of larger Pn-based or Tl/Pn-based clusters.

As mentioned above, the controlled preparation of binary Zintl anions containing atoms of different sizes from ternary Zintl solids of the form K_xTr/Tt_yPn_z remains a challenge – especially with regard to an efficient synthesis route.[10,13] Therefore, we aimed at gaining more insight in the extraction process in order to be able to ultimately design, optimize, and control the syntheses. Following this strategy, we successfully synthesized compounds comprising anions of two (widely) elusive elemental combinations, In/Sb and Tl/Sb, from ternary phases K_6InSb_3 and $K_6Tl_2Sb_3$. The structures of all new compounds were elucidated by means of single-crystal X-ray diffraction. The elemental compositions, which for In and Sb cannot be obtained from standard X-ray measurements, were determined by a combination of elemental analysis (micro-X-ray fluorescence spectroscopy, μ-XFS) and quantum chemical studies employing density functional theory (DFT) methods.

EXPERIMENTAL SECTION

General Synthesis Procedures. All procedures and reactions were executed under a dry argon atmosphere using standard Schlenk or glovebox techniques. Ethane-1,2-diamine (en) were distilled from CaH_2 and preserved over 3 Å molecular sieves, whereas toluene (tol) and 2-methoxy-2-methylpropane (MTBE) were distilled from sodium and stored over 3 Å molecular sieves. Before use, 4,7,13,16,21,24-hexaoxa-1,10-diazabicyclo[8.8.8]hexacosane (crypt-222) was vacuum-dried for a minimum of 18 h. All products show sensitivity toward air and moisture, but a reasonable thermal stability.

Syntheses. *K_6InSb_3 (**1**).* 0.848 g (21.70 mmol, 6.00 equiv) potassium, 0.831 g (7.23 mmol, 2.00 equiv) indium and 1.320 g (10.84 mmol, 3.00 equiv) antimony were placed in a tantalum ampule, which was closed by arc-welding in the glovebox. The tantalum ampule was placed in a fused silica ampule and flame-sealed under vacuum. Afterwards, the ampules were placed in a tube furnace, heated to 850 °C with 1.0 K min^{-1} and kept at this temperature for 10 h. The ampules were cooled down to 550 °C with 0.8 K min^{-1} and held at this temperature for 30.5 days. Afterwards, the oven was turned off. The reaction yield was 90.2% (2.707 g).

$K_6Tl_2Sb_3$. The compound was prepared according to a published protocol.[12] Details are given in the Supporting Information.

*$[K(crypt\text{-}222)]_2(InSb_3)\cdot en$ (**2**).* 200 mg (241.10 μmol, 1 equiv) of K_6InSb_3 and 546.5 mg (1.45 mmol, 6.02 equiv) of crypt-222 were placed in a Schlenk tube and were suspended in 12 mL en. The mixture was stirred for 1 h and 2 mL of the solution were filtered into a fresh Schlenk tube. Afterwards, it was layered by 3.5 mL toluene. After 10 d dark orange crystals had formed. The crystals were suitable for single crystal X-ray diffraction and could be identified as $[K(crypt\text{-}222)]_3(InSb_3)\cdot en$ (**2**).

*$[K(crypt\text{-}222)]_3(In_4Sb_5)\cdot 3tol$ (**3**).* 100 mg (120.55 μmol, 1.00 equiv) of K_6InSb_3 and 273.2 mg (725.73 μmol, 6.02 equiv) of crypt-222 were placed in a Schlenk tube and were suspended in 5 mL en. The reaction mixture was stirred for 21 h. Afterwards, the solution was filtered and divided in two Schlenk tubes and layered with 4 mL each toluene or MTBE and stored at 4 °C. After a few days the toluene layered solution showed some red block shaped crystals. The red crystals were suitable for single crystal X-ray diffraction and could be identified as $[K(crypt\text{-}222)]_3(In_4Sb_5)$ (**3**).

*Time-Dependent Extraction and Fractional Crystallization of $K_6Tl_2Sb_3$, and Synthesis of $[K(crypt\text{-}222)]_2(TlSb_3)\cdot en$ (**4**), $[K(crypt\text{-}222)]_3(Tl_4Sb_5)\cdot 3tol$ (**5**), $[K(crypt\text{-}222)]_2(TlSb_7)$ (**6**), and $[K(crypt\text{-}222)]_{4\infty}^{1}[(KSb_7)_2]$ (**7**).* 100 mg (99.10 μmol, 1.00 equiv) of $K_6Tl_2Sb_3$ and 224.7 mg (596.90 μmol, 6.02 equiv) of crypt-222 were placed in a Schlenk tube and suspended in 6 mL en. The first sample was filtered after 5 min into a second Schlenk tube and filled into a 250 μL Hamilton syringe. Mass spectrometry analyses (ESI(−)-MS) were performed immediately thereafter. Subsequently, the remaining filtrate was layered with 2 mL toluene and stored at 5 °C in a Schlenk tube. The process was repeated for the following samples in the respective order: 1, 4, 24 h and 1 week after the synthesis. The crystallization experiments after 1 h extraction time yielded black rhombohedral crystals of $[K(crypt\text{-}222)]_2(TlSb_7)$ (**6**). The experiment after 6 h yielded black rods of $[K(crypt\text{-}222)]_2(TlSb_3)\cdot en$ (**4**), while the experiment after 1 day of extraction time yielded black rods of $[K(crypt\text{-}222)]_4(KSb_7)$ (**7**) and black blocks of $[K(crypt\text{-}222)]_3(Tl_4Sb_5)\cdot 3tol$ (**5**). From the same reaction mixture, we were able to isolate another variant of compound **6**, denoted as compound **6a**, which crystallizes in the monoclinic space group $P2_1/c$ with three toluene solvent molecules per formula unit and four formula units per unit cell. Details are provided in the Supporting Information.

*Selective Synthesis of $[K(crypt\text{-}222)]_2(TlSb_3)\cdot en$ (**4**).* 100 mg (99.10 μmol, 1.00 equiv) of $K_6Tl_2Sb_3$ and 224.7 mg (596.90 μmol, 6.02 equiv) of crypt-222 were placed in a Schlenk tube and suspended in 7 mL en. The reaction mixture was stirred for 6 h at room temperature. The suspension was precipitated with 30 mL of toluene and stored at 5 °C for crystallization. The dark brown suspension was filtered using a PTFE tube with a glass fiber filter. The precipitate was conserved and dried under vacuum. Afterwards, a black, shiny powder was obtained (78 mg, 55.68 μmol, 56%).

https://doi.org/10.1021/acs.inorgchem.5c00724
Inorg. Chem. 2025, 64, 8711−8718

Scheme 2. Formation of Compounds 1−7 Illustrated by Non-Stoichiometric Reaction Schemes and Structural Diagrams of the (Molecular) Anions in 2−7 (Atom Assignment According to Quantum Chemical Calculations Detailed Below)[a]

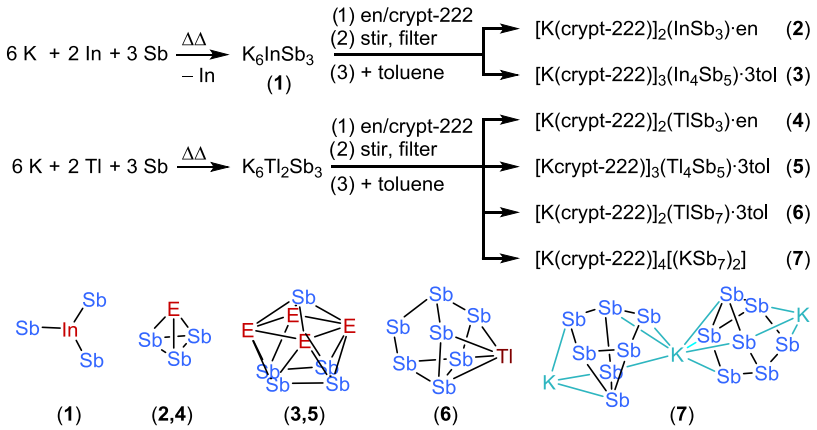

[a]Details on the synthesis procedures are given in the text and in the Experimental Section, the crystal structures and the computational results are shown and explained below and in the Supporting Information.

*Selective Synthesis of [K(crypt-222)]$_2$(Tl$_4$Sb$_5$)·3tol (**5**).* 100 mg (99.10 μmol, 1.00 equiv) of $K_6Tl_2Sb_3$ and 224.7 mg (596.9 μmol, 6,02 equiv) of crypt-222 were placed in a Schlenk tube and suspended in 3.5 mL en. The reaction mixture was stirred for 48 h at room temperature. While stirring a color change from dark brown-red to intense red was observed. The suspension was filtered using a PTFE tube with a glass fiber filter, due to the considerable amount of metallic residue present in the Schlenk tube. The dark red filtrate was layered with 4 mL toluene and stored at 5 °C. After 6 days black rhombohedral crystals of $[K(crypt\text{-}222)]_3Tl_4Sb_5$ (**5**) were obtained.

Micro-X-ray Fluorescence Spectroscopy. The measurements were performed on single crystals with a Bruker M4 Tornado and in one case with a Horiba XGT-9000, both equipped with a Rh-target X-ray tube, poly capillary optics and a Si drift detector. The emitted fluorescence photons were detected with an acquisition time of 180 s. Quantification of the elements is achieved through deconvolution of the spectra.

Electrospray-Ionization (ESI) Mass Spectrometry. All mass spectra were recorded on a Thermo Fisher Scientific Finnigan LTQ-FT spectrometer in negative-ion mode. In order to explore the possible formation pathway, we prepared a series of reaction solutions of the reaction leading to the compounds **2** and **3** in en. The reaction solutions were allowed to stir for 5, 30 min, 3 h, 1 day, 1 week and 2 weeks, before the measurements. The solutions were injected into the spectrometer with gastight 250 μL Hamilton syringes by syringe pump infusion. All capillaries within the system were washed with a dry en/toluene mixture (1:1) 2 h before and at least 10 min in between measurements to avoid decomposition reactions and consequent clogging. ESI parameters: Spray Voltage: 3.6 kV, Capillary Temp: 290 °C, Capillary Voltage: −20 kV, Tube lens Voltage: −121.75 kV, Sheath Gas: 45, Sweep Gas: 0, Auxiliary Gas: 40. Note that, while some of the species that were detected in ESI-MS were crystallized, for those that were not obtained in condensed phase, it cannot be excluded that they are generated under ESI-MS conditions only.

Single Crystal X-ray Diffraction. For the general procedure see the Supporting Information for details on the individual compounds. All compounds are very sensitive to moisture and air. A small number of crystals was extracted directly from the mother liquor into predried NVH oil. The data was collected at 180 K using different diffractometers (see the Supporting Information for the individual compounds). Structure solution (ShelXT)[14] and refinement (ShelXL)[15] were performed in Olex2.[16] The figures were made in Diamond4[17] using displacement ellipsoids with a probability of 50%.

Powder X-ray Diffraction. The data was collected on a Stoe StadiMP diffractometer system equipped with a Mythen 1 K silicon strip detector and Cu−Kα radiation (λ = 1.54056 Å). The samples were filled into glass capillaries (0.3 mm diameter), which were sealed airtight with soft wax. The tube was then mounted onto the goniometer head using wax (horizontal setup) and rotated throughout the measurement.

Quantum Chemical Studies. Computational studies were conducted by using the program system TURBOMOLE V7.7.1[18−20] and employing DFT methods. We used the meta-GGA functional TPSS[21] and dhf-TZVP basis sets[22] with effective core potentials (ECPs) at the In, Tl, and Sb atoms.[23−25] The Resolution-of-the-Identity (RI)[26] approximation with corresponding auxiliary bases[27] was used to speed up the calculations. The negative charges were compensated via COSMO.[28,29] The electronic structure was studied by means of population analyses.[30,31] Localized molecular orbitals were calculated according to Boys' method.[32] More details and supporting figures are given in the Supporting Information.

RESULTS AND DISCUSSION

The first challenge was to find suitable ternary phases to be extracted. Only one ternary phase has been described for the K/Tl/Sb system so far, $K_6Tl_2Sb_3$,[12] and only a few solids have been known for the combination of A/In/Sb (A = alkali metal), $A_2In_2Sb_3$ (A = K, Rb, Cs),[33−35] $K_{10}In_5Sb_9$,[36] $K_4In_4Sb_6$,[37] $Na_2In_2Sb_3$,[38] Na_3InSb_2[39] and $CsInSb_2$[40] as well as $Cs_8In_{27}Sb_{19}$.[41] We successfully reproduced $K_6Tl_2Sb_3$, but the same reaction conditions applied to the elemental combination of K/In/Sb afforded the new compound K_6InSb_3 (**1**), exhibiting a yet unprecedented A/In/Sb ratio, as probed by SCXRD, PXRD and μ-XFS.

The formation of the solid phases $K_6Tl_2Sb_3$ and **1**, as well as the syntheses of compounds **2** − **7**, comprising molecular anions, by extraction of the solids are summarized in Scheme 2. All compounds were obtained in single-crystalline form with yields varying between 5 and 70% with respect to Sb.

Compound **1** crystallizes in the triclinic space group $P\bar{1}$ with eight formula units in the unit cell. Views of the crystal structure are shown in Figure 1.

The structure of **1** is not related to that of $K_6Tl_2Sb_3$, in which the heteroatomic anionic unit consists of $^1_\infty[(Tl_4Sb_6)^{12-}]$ chains, but to that of recently reported $K_{12}Ge_{3.5}Sb_6$.[10] It is therefore based on carbonate-like $[InSb_3]^{6-}$ anions (Figure 1a) surrounded by K^+ ions with no connectivity between the anionic units. Similar $[AB_3]^{q-}$ anions have been reported for the lighter homologs $[SiP_3]^{5-}$, $[SiAs_3]^{5-}$, $[GeP_3]^{5-}$, $[GeAs_3]^{5-}$, and $[SnAs_3]^{5-}$.[42] In contrast to $K_{12}Ge_{3.5}Sb_6$, however, **1** is a

https://doi.org/10.1021/acs.inorgchem.5c00724
Inorg. Chem. 2025, 64, 8711−8718

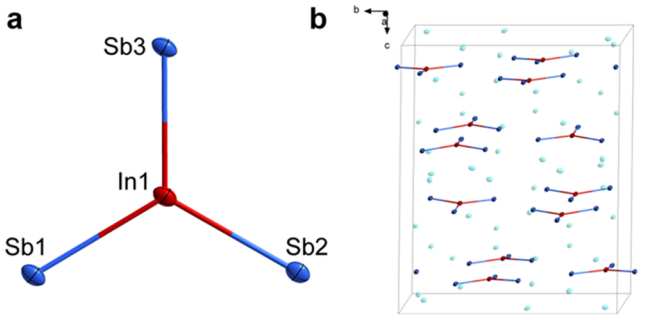

Figure 1. (a) Molecular structure of the carbonate-like $[InSb_3]^{6-}$ anion in K_6InSb_3 (**1**). (b) Extended unit cell of **1**. Thermal ellipsoids are shown at the 50% probability level. Selected interatomic distances [Å] and angles [°]: In1−Sb1 2.7644(7) − 2.8268(7), K···Sb 3.4461(17) − 4.159(2); Sb1−In1−Sb2 119.20(2)°; Sb1−In1−Sb3 120.77(2)°; Sb2−In1−Sb3 120.00(2)°. More structural details are provided in Figures S75−S77.

single-phase solid. This well-defined composition makes the phase a very good starting material for the synthesis of (soluble) $(InSb_3)^{2-}$ anions by partial oxidation of the $[InSb_3]^{6-}$ units during treatment with a corresponding solvent that allows for oxidative extraction according to previous reports. Ethane-1,2-diamine (en) was proven suitable in many instances, as it is sufficiently polar and simultaneously acts as an oxidant under release of H_2.[10,43−46]

We therefore extracted **1** with en and crypt-222 for 1 h. The expected binary *pseudo*-tetrahedral anion $(InSb_3)^{2-}$ was formed and could be isolated in the compound $[K(crypt\text{-}222)]_2(InSb_3)\cdot en$ (**2**) upon layering with toluene. Notably, if the extraction time is extended to 21 h, the oxidation proceeds, forming the nine-atom monocapped square-antiprismatic anion $(In_4Sb_5)^{3-}$. It was isolated as its $[K(crypt\text{-}222)]^+$ salt, $[K(crypt\text{-}222)]_3(In_4Sb_5)\cdot 3tol$ (**3**).

A corresponding extraction of the double-salt $K_6Tl_2Sb_3$ yielded a variety of products: $[K(crypt\text{-}222)]_2(TlSb_3)\cdot en$ (**4**), $[K(crypt\text{-}222)]_3(Tl_4Sb_5)\cdot 3$ tol (**5**), $[K(crypt\text{-}222)]_3(TlSb_7)$ (**6**), and $[K(crypt\text{-}222)]^{1}_{4\infty}[(KSb_7)_2]$ (**7**). The phase was prepared as per the previously published procedure with en and crypt-222. In situ monitoring of the extraction process by ESI-MS (SI, Figures S21−S73) indicated the formation of the $(TlSb_3)^{2-}$ anion in **4** to occur first, followed by the formation of the $(Tl_4Sb_5)^{3-}$ anion in **5**. The crystal structures of compounds **2** − **7** are illustrated in Figures 2 and 3.

Compounds **2** and **4** crystallize isotypically in the monoclinic space group $P2_1$ with two formula units in the unit cell. The *pseudo*-tetrahedral anions in these salts represent the missing examples of the $(TrPn_3)^{2-}$ series with elements of periods 5 and 6 (Tr = In, Tl; Pn = Sb, Bi). For the $(InSb_3)^{2-}$ anion in **2** (Figure 2a), the atom assignment based on X-ray analysis is not possible owing to the similar atomic numbers of the two elements. All four position were therefore refined with mixed sites occupancy (0.25 In, 0.75 Sb). The interatomic distances are between 2.8161(18) and 2.9568(27) Å. As expected, the bonds are slightly shorter compared to the heavier homolog $(InBi_3)^{2-}$.[47] In the $(TlSb_3)^{2-}$ anion in **4** (Figure 2c), three atoms (Tl1, Sb2 and Sb3) show elemental disorder (0. 33 In, 0.67 Tl), while the Sb4 position was refined as Sb only. The Tl/Sb−Sb/Tl distances are 2.8604(3) − 3.0194(31) Å − thus, between those in the heavier Bi/Tl homolog $(TlBi_3)^{2-}$ [9] and those in **2**, as expected. To account for the disorder of atomic positions in the figures, the

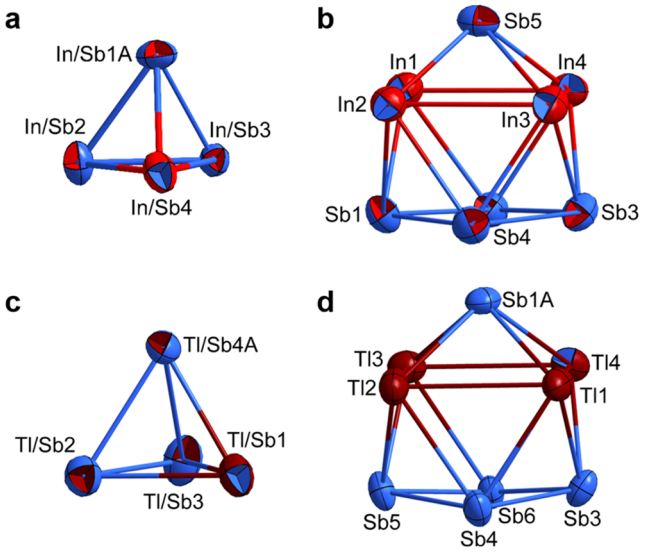

Figure 2. (a) Molecular structure of the $(InSb_3)^{2-}$ anion in **2** (disregarding disorder of some of the atoms); interatomic distances [Å]: In/Sb−In/Sb 2.8161(18) − 2.9568(27). (b) Molecular structure of the $(In_4Sb_5)^{3-}$ anion in **3**; selected interatomic distances [Å]: In−Sb 2.9270(13) − 3.0743(10), Sb−Sb 2.8509(14) − 2.9036(13), In−In 3.3811(13) − 3.5881(15). (c) Molecular structure of the $(TlSb_3)^{2-}$ anion in **4** (without disordered atom); interatomic distances [Å]: Tl/Sb−Sb/Tl 2.8604(3) − 3.0194(31). (d) Molecular structure of the $(Tl_4Sb_5)^{3-}$ anion in **5**; selected interatomic distances [Å]: Tl−Sb 2.9217(43) − 3.256(6), Sb−Sb 2.8123(11) − 3.0324(9), Tl−Tl 3.4443(8) − 3.6930(9). The thermal ellipsoids are drawn with 50% probability. More structural details are provided in Figures S78−S93.

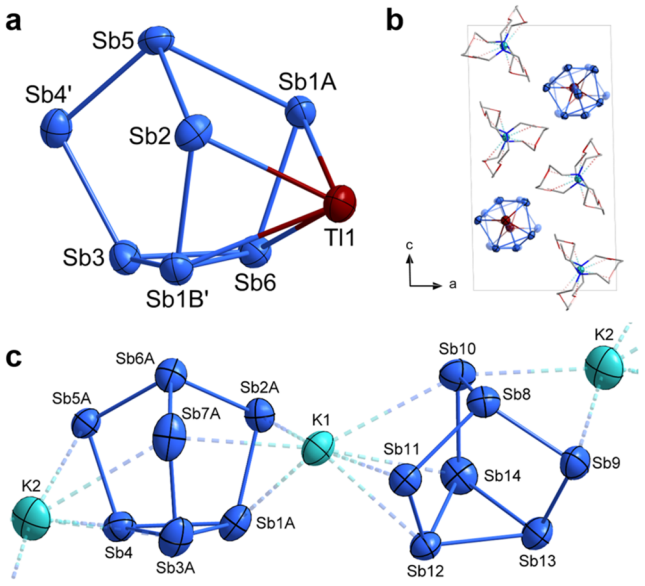

Figure 3. (a) Molecular structure of one of the two disordered positions of the $(TlSb_7)^{2-}$ anion in **6**; selected interatomic distances [Å]: Tl−Sb 3.189(3) − 3.283(3), Sb−Sb 2.416(4) − 3.229(2). (b) View of the crystal structure of **6**. (c) Cut-off from the one-dimensional $\{KSb_7\}^{2-}$ chain present in the crystal structure of **7**; selected interatomic distances [Å]: Sb−Sb 2.574(4) − 2.921(6). Thermal ellipsoids are drawn with 50% probability. More structural details are provided in Figures S94−S105.

respective atoms are drawn as octants with two colors, where the outer color indicates the atom type that is more probable on this atomic position based on the DFT studies discussed

https://doi.org/10.1021/acs.inorgchem.5c00724
Inorg. Chem. 2025, 64, 8711−8718

below. We would like to emphasize that all *pseudo*-tetrahedral binary anions are isoelectronic to neutral P_4 or As_4 molecules, which is why they are traditionally viewed as being composed of three Pn^0 atoms and one Tr^{2-} atom in case of the $(TrPn_3)^{2-}$ species. However, as we show below, quantum chemical calculations strongly suggest another charge distribution, which is more pointing toward a distribution of the negative charge over all four atoms. Notably, this leads to the same overall charge, and equally affords $a \pm 2$ difference in (formal) atomic charges. Beyond this background, we will discuss alternate interpretations of the other anions, as well.

Compounds **3** and **5** crystallize isotypically in the triclinic space group $P\bar{1}$ with two formula units in the unit cell. The $(In_4Pn_5)^{3-}$ anions in **3** and **5** are *nido*-type nine-atom cages (monocapped square-antiprisms). This structural motif is well-known from the homoatomic Zintl anions Tt_9^{4-} (Tt = group 14 atom)[48] and the isoelectronic cations Pn_9^{5+} (Pn = Sb, Bi)[49,50] as well as from homologous heteroatomic anions $(In_4Bi_5)^{3-}$ and $(Tl_4Bi_5)^{3-}$,[51,52] all of which have the same (40) valence electron count. The anions in **3** and **5** hence complement the series of this anion type with elements of periods 5 and 6 (Tr = In, Tl; Pn = Sb, Bi), which may be viewed as variations of the Pn_9^{5+} cations, in which four of the Pn atoms are replaced by isoelectronic Tr^{2-} − in agreement with the 3− total charge of the binary species. Alternatively (and in better agreement with the computational studies described below), it can be derived from Tt_9^{4-} in the following way: Four Tr and four Pn atoms in $(Tr_4Pn_5)^{3-}$ together provide the same electron count as eight Tt atoms in Tt_9^{4-}, while the ninth Tt atom is replaced by isoelectronic Pn^+, which compensates one of the four negative charges of the parent species. As expected, the interatomic distances in the four anions of the $(Tr_4Pn_5)^{3-}$ series develop according to the atomic sizes of the involved atoms: 2.8509(14) − 3.5881(15) Å for the $(In_4Sb_5)^{3-}$ anion in **3** (including all types of bonds), 2.8123(11) − 3.6930(9) Å for the $(Tl_4Sb_5)^{3-}$ anion in **5**, 3.008(4) − 3.818(4) Å in $(In_4Bi_5)^{3-}$,[51] and 3.0400(6) − 3.6386(5) Å in $(Tl_4Bi_5)^{3-}$.[9] Notably, the basal four-membered ring ({Sb_4} according to DFT calculations, see below) shows a more distinct distortion in the $(Tl_4Sb_5)^{3-}$ anion of **4** (Sb−Sb diagonals: 4.2114(9) and 4.0189(10) Å; folding angle 167.1°) than the {Sb_4} unit in the $(In_4Sb_5)^{3-}$ anion in **2** (Sb−Sb diagonals: 4.1049(12) and 4.0220(13) Å; folding angle 175.0°). At first glance, one might attribute this to the better match of In and Sb atoms in terms of their radii, but for $(In_4Bi_5)^{3-}$ and $(Tl_4Bi_5)^{3-}$, it was the Tl/Bi species that showed the larger distortion, although the sizes of Tl and Bi atoms are nearly identical.[9,51] We therefore assume that the four large Tl atoms force each four-membered ring attached to them to fold.

Compound **6** crystallizes in the monoclinic space group $P2/n$ with one formula unit in the unit cell. The anion in **6** is a monocapped nortricyclane-type {Sb_7} cage, with a Tl atom connected to the cage in an η^4-type fashion by one of its quadrangular faces. In the crystal, the anion is rotationally disordered (50:50). The molecular structure of one of these positions is shown in Figure 3a, a view of the crystal structure including the disorder is given in Figure 3b. Compound **7** crystallizes in the monoclinic space group $P2_1/c$ with two formula units in the unit cell, represented by two individual clusters and their corresponding K^+ ions (Figure 3c).

The attachment of a Tl atom to the {Sb_7} cage in compound **6** affects the Sb−Sb distances in it. The Sb1B'−Sb6 bond in the triangular base of the seven-atom cage facing the Tl atom (3.096(3) Å) is much longer than the two other bonds within the triangle (2.799(4) and 2.807(2) Å), which in turn are shorter than the corresponding Sb−Sb bonds in the bare Sb_7^{3-} anion (2.876(2) − 2.906(2) Å).[53] In agreement with the quantum chemical studies, the Tl atom should be viewed as a Tl^+ cation that is coordinated by the Sb_7^{3-} unit; indeed, regarding the Tl atoms as Tl^{2-} would require all Sb atoms to be formally neutral, which is not reflected in any structural detail of the anion. The Sb−Tl distances in **6** (3.189(3) − 3.283(3) Å) are by more than 0.3 Å longer than in **4**, in agreement with weaker and more ionic bonds. Additionally, the distances of the apical atom are elongated while the Sb−Sb bond on the opposite side of the Tl atom is shortened. The findings are consistent with the observation made for another cluster based on the coordination of a metal atom by Sb_7^{3-}, $[Sb_7\{Mo(CO)_3\}]^{3-}$,[54] featuring the same coordination mode. In $[Rb([2.2.2]crypt)]_4(Sb_{14}Zn)\cdot 8NH_3$ however,[55] another coordination mode of the Sb_7^{3-} unit is observed, with only two of the (formally negatively charged) μ-Sb atoms involved, and consequently, the Sb−Sb distances are significantly less affected.[46] The anion in compound **6** confirms the coordination found in isostructural anions $(TlP_7)^{3-}$ and $(TlAs_7)^{3-}$.[56] From the same reaction mixture, we were able to isolate another variant of compound **6**, denoted as compounds **6a**, which crystallizes in the monoclinic space group $P2_1/c$ with three toluene solvent molecules per formula unit and four formula units per unit cell. Details are provided in the Supporting Information.

Although being formally related in that a monocharged cation is coordinated by an Sb_7^{3-} anion, the anionic substructure of compound **7** is different from that in **6**. It does not form a molecular entity, but assembles into one-dimensional strands of alternating Sn_7^{3-} anions and K^+ cations; the remaining negative charge is compensated by two $[K(crypt\text{-}222)]^+$ complexes per formula unit which are more distant in the crystal structure. In contrast to the observations described for the $(TlSb_7)^{2-}$ molecule, the {Sb_7} cages in **7** are nearly unaffected by their coordination activity, which is alternatingly η^3-type and η^4-type, like in a closely related salt that crystallizes together with an NH_3 solvent molecule.[57] The Sb−Sb distances (2.574(4) − 2.921(6) Å) therefore compare well with those observed in the bare Sb_7^{3-} anion.[53] We assume that the formation of a coordination polymer is favored over isolated cages by a gain in energy; this might be even larger by covalent linkage, but to the best of our knowledge extended 1D, 2D, or 3D assemblies of {Sb_7} units have not been observed to date.

As mentioned above, normal X-ray diffraction experiments do not allow to distinguish between In and Sb atoms. To further analyze the experimental results, we therefore performed DFT studies. Details of the computational procedure are given in the Experimental Section and in the Supporting Information. The calculated bond lengths and angles were found to be in excellent agreement with the experimental values (Tables S17, S19, S21, S23, and S25). We therefore went on to analyze the electronic structures of the binary anions in compounds **2**−**6**.

As already shown in a previous study,[6] we only found 2-center 2-electron (2c2e) bonds within the *pseudo*-tetrahedral anions in **2** and **4** through inspection of localized molecular orbitals (LMOs, Figures S109 and S113). Population analyses showed polarization toward the Sb atoms, which is equivalent with a significant accumulation of negative charge on the Sb

https://doi.org/10.1021/acs.inorgchem.5c00724
Inorg. Chem. 2025, 64, 8711−8718

atoms. This tendency is more pronounced in the Tl/Sb case, supporting a much less pronounced charge distribution, rather towards Tr^{+} and Sb^{-} than Tr^{2-} and Sb^{0} as suggested by the *pseudo*-element concept, although population analyses (both Mulliken and NPA) suggest a slightly negative charge for the Tr atoms, too.

To verify the distribution of the In atoms in **3** and of the Tl atoms in **5**, respectively, we permutated both atom types over all possible positions. The most probable conformers are the ones depicted in Figure 2 above. All further isomers exhibit significantly higher relative energies compared to the global minimum structures. We can therefore conclude that only one isomer is present in the crystal in these two cases – which in the case of some of the anions discussed herein can undergo rotational disorder though. An overview over the most reasonable minima with the respective relative energies are given in Figures S112 and S119. While we again find 2c2e Sb–Sb bonds, all heteroatomic bonds represent 3c2e interactions (Figures S113 and S120), as expected for these Wade-Mingos-type cages. As in the *pseudo*-tetrahedral anions, the negative charge is distributed over the whole molecule with most electron density being situated on the Sb atoms.

The calculated bond lengths and angles in the anion in **6** were again in good agreement with the experimental values (Table S25). Another local minimum structure, where the Tl atom is bridging the trigonal Sb base of the nortricyclane-like parent motif (Figure S123), was found to be 90 kJ/mol higher in energy with respect to the global minimum structure, which is actually the one found in the crystal structure. Analysis of the canonical molecular orbitals (Figure S125) indicates the presence of cluster orbitals, as exemplified for some of the MOs in Figure 4. These MOs can be localized within the nortricyclane-like $\{Sb_7\}$ parent motif into regular 2c2e bonds, while the heteroatomic Tl1–Sb1 and Tl1–Sb2 bonds are strongly polarized toward the respective Sb atoms. This is in perfect agreement with the description of an Sb_7^{3-} cage coordinating a Tl^{+} cation; indeed, for this cluster, the Tl atom shows a slightly positive charge according to population analyses. Additionally, the localization procedure yields one 3-center-2-electron (3c2e) bond between Sb6, Sb7 and Tl1. The contribution coming from the Tl atom is small, however (Figure S124), thus supporting the relatively weak interaction in this part of the molecule and rationalizing the elongated Tl–Sb bonds.

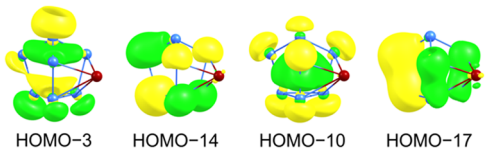

Figure 4. Examples for cluster orbitals in the anion of compound **6**, being of f-type (HOMO−3), d-type (HOMO−14), p-type (HOMO−10), and s-type (HOMO−17), respectively.

CONCLUSIONS

This study has allowed us to demonstrate that quantum chemical prediction is helpful in searching for yet missing examples of *pseudo*-tetrahedral binary anions of p-block (semi)metals. We have added two new anions to the library of these compounds, and established protocols for their targeted synthesis. Using time-dependent mass spectrometry and fractional crystallization revealed that the extraction reaction initially produces smaller anions in solution, which gradually evolve into larger ones over time by partial oxidation. This allowed for the isolation and characterization of a total of seven new compounds. Both the structure elucidation and concomitant quantum chemical calculations highlighted a subtle, yet important, impact of substituting In with Tl atoms on the bonding, resulting in slightly weaker heteroatomic bonds. The studies also indicated that in the Tr/Sb elemental combination, it is more reasonable to undertake a formal charge separation into Tr^{+} and Sb^{-}, although contradicting the widely applied *pseudo*-element concept. Future research aims to utilize these new binary anions in reactions involving d- and f-block elements to explore their reactivity differences. Additionally, we plan to expand the collection of *pseudo*-tetrahedral cluster anions with different combinations of elements.

ASSOCIATED CONTENT

Supporting Information

The Supporting Information is available free of charge at https://pubs.acs.org/doi/10.1021/acs.inorgchem.5c00724.

Crystallographic information on **1**–**7**, details on the syntheses, single crystal X-ray diffraction data, powder X-ray diffraction data, X-ray fluorescence spectroscopy, mass spectrometry data, and quantum chemical calculations (PDF)

Calculated_Coordinates (TXT)

Accession Codes

Deposition Numbers 2424158–2424164 and 2424168 contain the supporting crystallographic data for this paper. These data can be obtained free of charge via the joint Cambridge Crystallographic Data Centre (CCDC) and Fachinformationszentrum Karlsruhe Access Structures service.

AUTHOR INFORMATION

Corresponding Author

Stefanie Dehnen – *Karlsruhe Institute of Technology, Institute of Nanotechnology, 76131 Karlsruhe, Germany;* orcid.org/0000-0002-1325-9228; Email: stefanie.dehnen@kit.edu

Authors

Katrin Beuthert – *Karlsruhe Institute of Technology, Institute of Nanotechnology, 76131 Karlsruhe, Germany;* orcid.org/0000-0002-8334-6212

Nils Spang – *Karlsruhe Institute of Technology, Institute of Nanotechnology, 76131 Karlsruhe, Germany*

Diana Carolina Alzate Millan – *Fachbereich Chemie und Wissenschaftliches Zentrum für Materialwissenschaften (WZMW), Philipps–Universität Marburg, 35043 Marburg, Germany*

Lukas Guggolz – *Karlsruhe Institute of Technology, Institute of Nanotechnology, 76131 Karlsruhe, Germany*

Complete contact information is available at: https://pubs.acs.org/10.1021/acs.inorgchem.5c00724

Author Contributions

The manuscript was written through contributions of all authors. All authors have given approval to the final version of the manuscript.

https://doi.org/10.1021/acs.inorgchem.5c00724
Inorg. Chem. 2025, 64, 8711–8718

Notes

The authors declare no competing financial interest.

■ ACKNOWLEDGMENTS

The authors gratefully acknowledge financial support from the Deutsche Forschungsgemeinschaft (DFG, German Research Foundation) through the Collaborative Research Centre "4f for Future" (CRC 1573, project number 471424360), project A4. We would like to thank Dieter Fenske for help with the single crystal measurements, Jan Bamberger as well as Franziska Ganslmeier for the measurement of the mass spectra, and Mika Siemonsen for assistance with the synthesis of the In/Sb compounds. We acknowledge support by the state of Baden-Württemberg through bwHPC and the German Research Foundation (DFG) through grant no INST 40/575-1 FUGG (JUSTUS 2 cluster). We acknowledge the support provided through the Centre of Excellence on Molecular Materials and Functions under the Institution of Eminence scheme of IIT Madras, India, and we acknowledge support by the Karlsruhe Nano-Micro Facility, KNMFi.

■ REFERENCES

(1) Scharfe, S.; Kraus, F.; Stegmaier, S.; Schier, A.; Fässler, T. F. Zintl Ions, Cage Compounds, and Intermetalloid Clusters of Group 14 and Group 15 Elements. *Angew. Chem., Int. Ed.* **2011**, *50*, 3630−3670.

(2) Wilson, R. J.; Weinert, B.; Dehnen, S. Recent developments in Zintl cluster chemistry. *Dalton Trans.* **2018**, *47*, 14861−14869.

(3) Townrow, O. P. E.; Chung, C.; Macgregor, S. A.; Weller, A. S.; Goicoechea, J. M. A Neutral Heteroatomic Zintl Cluster for the Catalytic Hydrogenation of Cyclic Alkenes. *J. Am. Chem. Soc.* **2020**, *142*, 18330−18335.

(4) Xu, Y.-H.; Tian, W.-J.; Muñoz-Castro, A.; Frenking, G.; Sun, Z.-M. An all-metal fullerene: $[K@Au_{12}Sb_{20}]_5$. *Science* **2023**, *382*, 840−843.

(5) Peerless, B.; Schmidt, A.; Franzke, Y. J.; Dehnen, S. φ-Aromaticity in prismatic {Bi_6}-based clusters. *Nat. Chem.* **2023**, *15*, 347−356.

(6) Guggolz, L.; Dehnen, S. Systematic DFT Studies on Binary Pseudo-tetrahedral Zintl Anions: Relative Stabilities and Reactivities towards Protons, Trimethylsilyl Groups, and Iron Complex Fragments. *Chem. - Eur. J.* **2020**, *26*, 11819−11828.

(7) Wilson, R. J.; Hastreiter, F.; Reiter, K.; Büschelberger, P.; Wolf, R.; Gschwind, R.; Weigend, F.; Dehnen, S. $[Co@Sn_6Sb_6]^{3-}$: An Off-Center Endohedral 12-Vertex Cluster. *Angew. Chem., Int. Ed.* **2018**, *57*, 15359−15363.

(8) Xu, L.; Sevov, S. C. Heteroatomic Deltahedral Clusters of Main-Group Elements: Synthesis and Structure of the zintl Ions $[In_4Bi_5]^{3-}$, $[InBi3]^{2-}$, and $[GaBi3]^{2-}$. *Inorg. Chem.* **2000**, *39*, 5383−5389.

(9) Lichtenberger, N.; Spang, N.; Eichhöfer, A.; Dehnen, S. Between localization and delocalization: $Ru(cod)^{2+}$ units in the zintl clusters $[Bi_9\{Ru(cod)\}_2]^{3-}$ and $[Tl_2Bi_6\{Ru(cod)\}]^{2-}$. *Angew. Chem., Int. Ed.* **2017**, *56*, 13253−13258.

(10) Beuthert, K.; Pan, F.; Guggolz, L.; Wilson, R. J.; Hempelmann, J.; Dronskowski, R.; Dehnen, S. Between Elemental Match and Mismatch: From $K_{12}Ge_{3.5}Sb_6$ to Salts of $(Ge_2Sb_2)^{2-}$, $(Ge_4Sb_{12})^{4-}$, and $(Ge_4Sb_{14})^{4-}$. *Angew. Chem., Int. Ed.* **2022**, *61*, No. e202207232.

(11) Liu, C.; Tkachenko, N. V.; Popov, I. A.; Fedik, N.; Min, X.; Xu, C.-Q.; Li, J.; McGrady, J. E.; Boldyrev, A. I.; Sun, Z.-M. Structure and Bonding in $[Sb@In_8Sb_{12}]^{3-}$ and $[Sb@In_8Sb_{12}]^{5-}$. *Angew. Chem., Int. Ed.* **2019**, *58*, 8367−8371.

(12) Chi, L.; Corbett, J. D. K6Tl2Sb3, A Zintl Phase with a Novel Heteroatomic $[Tl_4Sb_6^{12-}]$ Chain. *Inorg. Chem.* **2001**, *40*, 2705−2708.

(13) Lichtenberger, N.; Franzke, Y. J.; Massa, W.; Weigend, F.; Dehnen, S. The Identity of "Ternary" A/Tl/Pb or K/Tl/Bi Solid Mixtures and Binary Zintl Anions Isolated From Their Solutions. *Chem. - Eur. J.* **2018**, *24*, 12022−12030.

(14) Sheldrick, G. M. SHELXT - Integrated space-group and crystal-structure determination. *Acta Crystallogr., Sect. A:Found. Adv.* **2015**, *71*, 3−8.

(15) Sheldrick, G. M. Crystal structure refinement with SHELXL. *Acta Crystallogr., Sect. C:Struct. Chem.* **2015**, *71*, 3−8.

(16) Dolomanov, O. V.; Bourhis, L. J.; Gildea, R. J.; Howard, J. A. K.; Puschmann, H. OLEX2: a complete structure solution, refinement and analysis program. *J. Appl. Crystallogr.* **2009**, *42*, 339−341.

(17) Dr. H. Putz & Dr. K. Brandenburg GbR. Diamond − Crystal and Molecular Structure Visualization, Crystal Impact. http://www.crystalimpact.com/diamond.

(18) Eichkorn, K.; Treutler, O.; Öhm, H.; Häser, M.; Ahlrichs, R. Auxiliary basis sets to approximate Coulomb potentials. *Chem. Phys. Lett.* **1995**, *240*, 283−290.

(19) Balasubramani, S. G.; Chen, G. P.; Coriani, S.; Diedenhofen, M.; Frank, M. S.; Franzke, Y. J.; Furche, F.; Grotjahn, R.; Harding, M. E.; Hättig, C.; Hellweg, A.; Helmich-Paris, B.; Holzer, C.; Huniar, U.; Kaupp, M.; Khah, A. M.; Khani, S. K.; Müller, T.; Mack, F.; Nguyen, B. D.; Parker, S. M.; Perlt, E.; Rappoport, D.; Reiter, K.; Roy, S.; Rückert, M.; Schmitz, G.; Sierka, M.; Tapavicza, E.; Tew, D. P.; van Wüllen, C.; Voora, V. K.; Weigend, F.; Wodyński, A.; Yu, J. M. TURBOMOLE: Modular program suite for ab initio quantum-chemical and condensed-matter simulations. *J. Chem. Phys.* **2020**, *152*, No. 184107.

(20) URBOMOLE V7.8 2024, a development of University of Karlsruhe and Forschungszentrum Karlsruhe GmbH, 1989−2007, TURBOMOLE GmbH. http://www.turbomole.com.

(21) Tao, J.; Perdew, J. P.; Staroverov, V. N.; Scuseria, G. E. Climbing the Density Functional Ladder: Nonempirical Meta−Generalized Gradient Approximation Designed for Molecules and Solids. *Phys. Rev. Lett.* **2003**, *91*, No. 146401.

(22) Weigend, F.; Ahlrichs, R. Balanced basis sets of split valence, triple zeta valence and quadruple zeta valence quality for H to Rn: Design and assessment of accuracy. *Phys. Chem. Chem. Phys.* **2005**, *7*, 3297−3305.

(23) Metz, B.; Stoll, H.; Dolg, M. Small-core multiconfiguration-Dirac−Hartree−Fock-adjusted pseudopotentials for post-d main group elements: Application to PbH and PbO. *J. Chem. Phys.* **2000**, *113*, 2563−2569.

(24) Metz, B.; Schweizer, M.; Stoll, H.; Dolg, M.; Liu, W. A small-core multiconfiguration Dirac−Hartree−Fock-adjusted pseudopotential for Tl − application to TlX (X = F, Cl, Br, I). *Theor. Chem. Acc.* **2000**, *104*, 22−28.

(25) Weigend, F.; Baldes, A. Segmented contracted basis sets for one- and two-component Dirac−Fock effective core potentials. *J. Chem. Phys.* **2010**, *133*, No. 174102.

(26) Eichkorn, K.; Weigend, F.; Treutler, O.; Ahlrichs, R. Auxiliary basis sets for main row atoms and transition metals and their use to approximate Coulomb potentials. *Theor. Chem. Acc.* **1997**, *97*, 119−124.

(27) Weigend, F. Accurate Coulomb-fitting basis sets for H to Rn. *Phys. Chem. Chem. Phys.* **2006**, *8*, 1057−1065.

(28) Schäfer, A.; Klamt, A.; Sattel, D.; Lohrenz, J. C. W.; Eckert, F. COSMO Implementation in TURBOMOLE: Extension of an efficient quantum chemical code towards liquid systems. *Phys. Chem. Chem. Phys.* **2000**, *2* (10), 2187−2193.

(29) Klamt, A.; Schüürmann, G. COSMO: a new approach to dielectric screening in solvents with explicit expressions for the screening energy and its gradient. *J. Chem. Soc., Perkin Trans. 2* **1993**, 799−805.

(30) Mulliken, R. S. Electronic Population Analysis on LCAO-MO Molecular Wave Functions. III. Effects of Hybridization on Overlap and Gross AO Populations. *J. Chem. Phys.* **1955**, *23*, 2338−2342.

(31) Reed, A. E.; Weinstock, R. B.; Weinhold, F. Natural Population Analysis. *J. Chem. Phys.* **1985**, *83*, 735−746.

(32) Boys, S. F. *Quantum Theory of Atoms, Molecules and the Solid State*; Löwdin, P.-O., Ed.; Academic Press: New York, 1966; pp 253−262.

https://doi.org/10.1021/acs.inorgchem.5c00724
Inorg. Chem. 2025, 64, 8711−8718

(33) Cordier, G.; Ochmann, H. Crystal structure of dipotassium phyllo-triantimonidodiindate. *Z. Kristallogr. - Cryst. Mater.* **1991**, *197*, 291−292.
(34) Gourdon, O.; Boucher, F.; Gareh, J.; Evain, M.; O'Connor, C. J.; Jin-Seung, J. Rubidium indium antimonide, $Rb_2In_2Sb_3$. *Acta Crystallogr., Sect. C:Cryst. Struct. Commun.* **1996**, *52*, 2963−2964.
(35) Blase, W.; Cordier, G.; Poth, L.; Weil, K. G. Crystal structure of dicaesium phyllo-triantimonidodiindate, $Cs_2In_2Sb_3$. *Z. Kristallogr. - Cryst. Mater.* **1995**, *210*, No. 60.
(36) Blase, W.; Cordier, G.; Somer, M. Crystal structure of decapotassium nonaantimonidopentaindate, $K_{10}In_5Sb_9$. *Z. Kristallogr. - Cryst. Mater.* **1993**, *203*, 146−147.
(37) Birdwhistell, T. L. T.; Klein, C. L.; Jeffries, T.; Stevens, E. D.; O'Connor, C. J. Synthesis and crystal structures of the layered I-III-V Zintl phases, $K_4In_4X_6$, where X= As, Sb. *J. Mater. Chem.* **1991**, *1*, 555−558.
(38) Cordier, G.; Ochmann, H. Crystal structure of disodium phyllo-triantimonidodiindate. *Z. Kristallogr. - Cryst. Mater.* **1991**, *197*, 281−282.
(39) Cordier, G.; Ochmann, H. Crystal structure of trisodium tecto-diantimonidoindate, Na_3InSb_2. *Z. Kristallogr.* **1991**, *195*, 107−108.
(40) Wang, J.; Owens-Baird, B.; Kovnir, K. From three-dimensional clathrates to two-dimensional Zintl phases $AMSb_2$ (A = Rb, Cs; M = Ga, In) composed of pentagonal M-Sb rings. *Inorg. Chem.* **2022**, *61*, 533−541.
(41) Owens-Baird, B.; Wang, J.; Wang, S. G.; Chen, Y.-S.; Lee, S.; Donadio, D.; Kovnir, K. III−V clathrate semiconductors with outstanding hole mobility. $Cs_8In_{27}Sb_{19}$ and $A_8Ga_{27}Sb_{19}$ (A = Cs, Rb). *J. Am. Chem. Soc.* **2020**, *142*, 2031−2041.
(42) Eisenmann, B.; Klein, J.; Somer, M. Anions Isosteric with CO in Cs_5SiP_3, Cs_5SiAs_3, Cs_5GeP_3, and Cs_5GeAs_3. *Angew. Chem., Int. Ed. Engl.* **1990**, *29*, 87−88.
(43) Weinert, B.; Müller, F.; Harms, K.; Clérac, R.; Dehnen, S. Origin and Location of Electrons and Protons during the Formation of Intermetalloid Clusters $[Sm@Ga_{3-x}H_{3-2x}Bi_{10+x}]^{3-}$ (x = 0, 1). *Angew. Chem., Int. Ed.* **2014**, *53*, 11979−11983.
(44) Weinert, B.; Eulenstein, A. R.; Ababei, R.; Dehnen, S. Formation of $[Bi_{11}]^{3-}$, A Homoatomic, Polycyclic Bismuth Polyanion, by Pyridine-Assisted Decomposition of $[GaBi_3]^{2-}$. *Angew. Chem., Int. Ed.* **2014**, *53*, 4704−4708.
(45) Perla, L. G.; Sevov, S. C. $[Bi_{12}Ni_7(CO)_4]^{4-}$: Aggregation of Intermetalloid Clusters by Their Thermal Deligation and Oxidation. *Inorg. Chem.* **2015**, *54*, 8401−8405.
(46) Lips, F.; Clérac, R.; Dehnen, S. $[Pd_3Sn_8Bi_6]^{4-}$: A 14-Vertex Sn/Bi Cluster Embedding a Pd_3 Triangle. *J. Am. Chem. Soc.* **2011**, *133*, 14168−14171.
(47) Xu, L.; Sevov, S. C. Heteroatomic Deltahedral Clusters of Main-Group Elements: Synthesis and Structure of the Zintl Ions $[In_4Bi_5]^{3-}$, $[InBi_3]^{2-}$, and $[GaBi_3]^{2-}$. *Inorg. Chem.* **2000**, *39*, 5383−5389.
(48) Corbett, J. D. Polyanionic Clusters and Networks of the Early p-Element Metals in the Solid State: Beyond the Zintl Boundary. *Angew. Chem., Int. Ed.* **2000**, *39*, 670−690.
(49) Ulvenlund, S.; Ståhl, K.; Bengtsson-Kloo, L. Structural and Quantum Chemical Study of Bi_5^{3+} and Isoelectronic Main-Group Metal Clusters. The Crystal Structure of Pentabismuth(3+) Tetrachlorogallate(III) Refined from X-ray Powder Diffraction Data and Synthetic Attempts on Its Antimony Analogue. *Inorg. Chem.* **1996**, *35*, 223−230.
(50) Hershaft, A.; Corbett, J. D. The Crystal Structure of Bismuth Subchloride. Identification of the Ion Bi_9^{5+}. *Inorg. Chem.* **1963**, *2*, 979−985.
(51) Xu, L.; Sevov, S. C. Heteroatomic deltahedral clusters of main-group elements: synthesis and structure of the Zintl ions $[In_4Bi_5]^{3-}$, $[InBi_3]^{2-}$, and $[GaBi_3]^{2-}$. *Inorg. Chem.* **2000**, *39*, 5383−5389.
(52) Lichtenberger, N.; Spang, N.; Eichhöfer, A.; Dehnen, S. Between Localization and Delocalization: Ru (cod) 2+ Units in the Zintl Clusters $[Bi_9\{Ru(cod)\}_2]^{3-}$ and $[Tl_2Bi_6\{Ru(cod)\}]^{2-}$. *Angew. Chem., Int. Ed.* **2017**, *56*, 13253−13258.
(53) Critchlow, S. C.; Corbett, J. D. Homopolyatomic Anions of the Post Transition-Elements − Synthesis and Structure of Potassium-Crypt Salts of the Tetraantimonide(2-) and Heptaantimonide(3-) Anions, Sb_4^{2-} and Sb_7^{3-}. *Inorg. Chem.* **1984**, *23*, 770−774.
(54) Bolle, U.; Tremel, W. Insertion of a Transition Metal Fragment into a Heptaantimonide(3-) Anion: Synthesis and Structure of $[Sb_7Mo(CO)_3]^{3-}$. *J. Chem. Soc., Chem. Commun.* **1994**, 217−219.
(55) Kaas, M.; Korber, N. Synthesis and Characterization of $[Rb([18]crown-6)]_3As_{15}Zn{\cdot}4NH_3$ and $[Rb([2.2.2]crypt)]_4Sb_{14}Zn{\cdot}8NH_3$. *Z. Anorg. Allg. Chem.* **2017**, *643*, 1331−1334.
(56) Knapp, C. M.; Large, J. S.; Rees, N. H.; Goicoechea, J. M. A versatile salt-metathesis route to heteroatomic clusters derived from phosphorus and arsenic Zintl anions. *Dalton Trans.* **2011**, *40*, 735−745.
(57) Zavalij, P. Y.; Stevensx, L. M.; Wang, Y.; Eichhorn, B. W. CCDC 1920986: Experimental Crystal Structure Determination. 2019 DOI: 10.5517/ccdc.csd.cc22gy9t.

https://doi.org/10.1021/acs.inorgchem.5c00724
Inorg. Chem. 2025, 64, 8711−8718